

Infrared Spectra and Structures of Silver–PAH Cation Complexes

Marco Savoca,[†] Torsten Wende,[‡] Ling Jiang,[‡] Judith Langer,[†] Gerard Meijer,[‡] Otto Dopfer,^{*,†} and Knut R. Asmis^{*,‡}

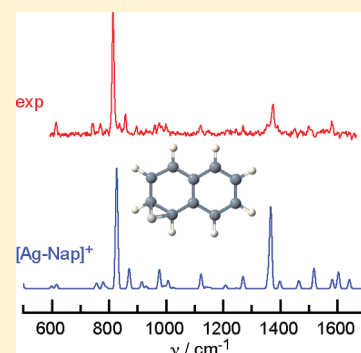
[†]Institut für Optik und Atomare Physik, Technische Universität Berlin, Hardenberstrasse 36, 10623 Berlin, Germany

[‡]Fritz-Haber-Institut der Max-Planck-Gesellschaft, Faradayweg 4-6, 14195 Berlin, Germany

S Supporting Information

ABSTRACT: Hybrids of metal atoms and polycyclic aromatic hydrocarbons (PAHs) are promising building blocks for new materials with tailored opto-electronic properties. We report the first experimental mid-infrared (550–1650 cm^{-1}) spectra of $[\text{Ag-PAH}]^+$ complexes measured in the linear absorption regime via messenger tagging of size-selected cryogenically cooled complexes. Infrared photodissociation (IRPD) spectra of $[\text{Ag-PAH}]^+ \cdot \text{Ne}$ complexes (PAH = naphthalene and azulene) are assigned on the basis of a comparison to simulated vibrational spectra from density functional calculations. The analysis of the IRPD spectra, which resolve IR bands as weak as a few km/mol , allows us to identify the Ag^+ binding site and to gain valuable insight into the effects of Ag^+ complexation on the geometry and charge distribution of the PAH.

SECTION: Dynamics, Clusters, Excited States



Polycyclic aromatic hydrocarbons (PAHs) are stable and unreactive species naturally occurring in oil, coal, and fossil fuels. They play a major role in pollution, combustion,¹ and interstellar chemistry.² Their two-dimensional extension, graphene,³ has promising electronic and mechanical properties,^{4,5} as appreciated by the Nobel prize in physics awarded in 2010. Hybrids composed of PAH (or graphene) and metal atoms (or metal clusters) are considered as potential targets for novel materials with tailored catalytic, electronic, optical, and magnetic properties.⁶ These can be tuned by variation of several parameters, such as metal type and cluster size, PAH size, charge state, and substitution of functional groups. In particular, transition metals can form strong coordinative bonds to PAHs due to donation of d electrons from the metal into the vacant π^* orbital of the PAH and back-donation of π electrons from the PAH into partially filled metal orbitals.⁷ The variation in interaction strength and geometry leads to different band gaps depending on the metal. Control and tuning of band gaps in molecular materials is one of the fundamental questions for designing molecular electronic devices. In contrast to metal–benzene complexes,^{7,8} little information is available about the geometric and electronic properties of metal–PAH complexes.^{9–12} During a recent measurement campaign, we recorded infrared photodissociation (IRPD) spectra of $[\text{Ag-(PAH)}_n]^+$ complexes with $n = 1$ and 2 and PAH = azulene (Azu), naphthalene (Nap), anthracene, phenanthrene, and pyrene in the fingerprint range (550–1650 cm^{-1}). Here, we report initial results on the structure and vibrational spectroscopy of size-selected $[\text{Ag-Azu}]^+ \cdot \text{Ne}$ and $[\text{Ag-Nap}]^+ \cdot \text{Ne}$ complexes (Figure 1).

In the present study, we apply a modern, generally applicable approach to obtain vibrational spectra of cold metal cation–PAH complexes in the linear absorption regime. Isolated complexes

are efficiently formed by electrospray ionization (ESI), as shown in Figure F1 in the Supporting Information (SI).^{13,14} A messenger atom, Ne in this case, is subsequently attached to collisionally cooled mass-selected $[\text{Ag-PAH}]^+$ ions in a 19 K ring electrode trap via three body collisions (Figure F1 in SI).^{15,16} All ions are then transferred from the trap into the extraction region of a time-of-flight (TOF) mass spectrometer, where they interact with tunable IR radiation of the Free Electron Laser for Infrared eXperiments (FELIX).^{17,18} IRPD spectra of cold $[\text{Ag-PAH}]^+ \cdot \text{Ne}$ complexes are obtained by analyzing the resonant vibrational photodissociation process as a function of the laser frequency (messenger technique):^{16,19–21}



As Ag^+ is a closed-shell transition-metal ion with $[\text{Kr}]4d^{10}5s^0$ configuration, predominantly electrostatic character of the cation– π interaction may be expected for $[\text{Ag-PAH}]^+$. However, due to similar ionization energies of Ag (IE = 7.58 eV) and the considered PAH molecules (IE = 7.42–8.14 eV),²² orbital interactions involving electron transfer of the type $\pi \rightarrow \text{Ag}^+$ (σ donation) and $\text{Ag}^+ \rightarrow \pi^*$ (π back-donation) influence both the energetic and structural parameters of the complex.^{7,23,24} As such orbital interactions provide a severe challenge for the quantum chemical description of these hybrid complexes, their experimental characterization is of importance.

Calculations at the B3LYP/aug-cc-pVTZ (vide infra) yield a single minimum on the $[\text{Ag-Nap}]^+$ potential (Figure 1), in

Received: July 8, 2011

Accepted: July 22, 2011

Published: July 29, 2011

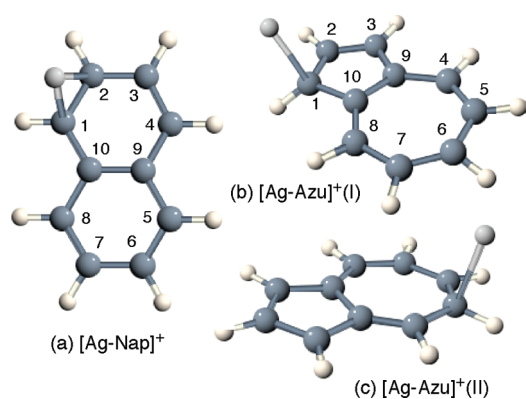


Figure 1. Optimized structures of [Ag-Nap]⁺, [Ag-Azu]⁺(I), and [Ag-Azu]⁺(II) obtained at the B3LYP/aug-cc-pVTZ level.

which Ag⁺ is located above the ring nearly symmetrically between C1 and C2, with a binding energy of $D_0 = 161$ kJ/mol (1.67 eV) and distances of 2.436 and 2.398 Å to C1 and C2, respectively. Detailed geometrical parameters are provided in Figure F2 in the SI. Furthermore, Ne and PAH bind to opposite sites of Ag⁺, in line with the preferred coordination number of 2 for Ag⁺.^{24,25} As the Ag⁺-Ne interaction (<10 kJ/mol)²⁶ is roughly 20 times weaker than the [Ag-PAH]⁺ interaction (~200 kJ/mol), the impact of Ne on the properties of [Ag-PAH]⁺ can be neglected, with vibrational frequency shifts of <2 cm⁻¹, as demonstrated in Figure F3 in the SI.

The IRPD spectrum of [Ag-Nap]⁺·Ne, measured in the 590–1650 cm⁻¹ range, is compared to various simulated linear absorption spectra in Figure 2. In the following, we assume that the measured photodissociation cross section σ is proportional to the calculated IR intensity.¹⁶ The experimental spectrum (Figure 2c) exhibits 21 sharp features labeled A–U, considerably more than predicted for neutral naphthalene (Figure 2a), confirming the symmetry lowering upon complexation with Ag⁺. The satisfactory agreement between the simulated IR spectrum of the minimum-energy structure (Figure 2b) and the measured IRPD spectrum (Figure 2c), particularly with regard to the peak positions, allows for an assignment of all transitions observed (Table T1 in SI). The maximum deviation between experimental and calculated frequencies is 23 cm⁻¹, with an average difference of 11 cm⁻¹. The high sensitivity of the present approach is evidenced by the detection of transitions as weak as 3 km/mol with a relatively high spectral resolution (<10 cm⁻¹). This is in contrast to previous IR multiple photon dissociation (IRMPD) spectra of Fe⁺-Nap,¹⁰ which display only the two most intense transitions occurring in this spectral range at 822 and 1352 cm⁻¹ with widths of ~50 cm⁻¹ due to the low sensitivity of the multiple photon absorption process and the high temperature of the ions (300 K).

The most intense feature E (814 cm⁻¹) in the experimental spectrum is assigned to a CH out-of-plane bending mode, which is calculated at 827 cm⁻¹ (ν_{30} , b_{1u}), that is, 31 cm⁻¹ shifted to the blue of the corresponding transition in bare Nap (796 cm⁻¹). The second most intense transition (Q) observed at 1374 cm⁻¹ is attributed to a CC stretching mode ($\nu_5 = 1367$ cm⁻¹, a_g). The corresponding transition in isolated Nap (1375 cm⁻¹) is forbidden but gains considerable intensity upon complexation with Ag⁺ (68 km/mol). Furthermore, the potential energy surface for Ag⁺ above the aromatic plane is relatively flat,^{23,27,28} with low

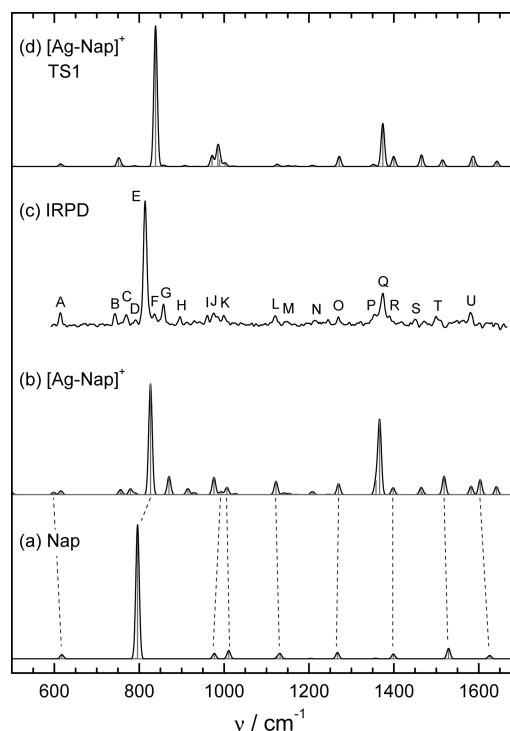


Figure 2. Simulated IR spectra of Nap (a), the global minimum-energy structure of [Ag-Nap]⁺ (b), and the lowest-energy transition state (TS1, Figure F4 in SI) (d) calculated at the B3LYP/aug-cc-pVTZ level (10 cm⁻¹ convolution) compared to the IRPD spectrum of [Ag-Nap]⁺·Ne (c). The vibrational assignments of the bands A–U are listed in Table T1 in the SI, along with frequencies and IR intensities of the calculated spectra.

barriers (<20 kJ/mol) for interconversion between equivalent minima. The IR spectra calculated for the minimum and the lowest-energy transition states (TS1 and TS2) connecting the four equivalent minima on the same side of Nap exhibit a pronounced sensitivity to the Ag⁺ binding site (Figures 2 and F4 in SI). While the simulated spectra assume ions at 0 K, the experimental spectra probe ions at a low but finite internal temperature. Consequently, the difference in the calculated and observed intensities for transition Q may reflect some delocalization of Ag⁺ in the ground vibrational state through zero-point motion and/or internal excitation of low-frequency intermolecular bending modes of the ions at finite T . Thus, the detailed experimental linear IR spectrum [Ag-Nap]⁺ provides a very sensitive probe for the position and degree of delocalization of Ag⁺ above the Nap plane, which can be analyzed in more detail in the future by multidimensional rovibrational calculations on sophisticated potential energy surfaces.

The two most intense transitions E (out-of-plane CH bend) and Q (CC stretch) in the experimental [Ag-Nap]⁺·Ne spectrum display frequency shifts of +34 and -6 cm⁻¹ upon Ag⁺ complexation. These modes exhibit larger shifts in the IRMPD spectrum of [Fe-Nap]⁺ (+42 and -28 cm⁻¹) due to the much stronger interaction in this complex (265 kJ/mol).¹⁰ These frequency shifts result from a distortion of the Nap geometry upon complexation. In more detail, the similar IE values of Ag (7.58 eV) and Nap (8.14 eV) give rise to partial electron transfer from Nap to Ag⁺ in the [Ag-Nap]⁺ complex; 0.1 e is predicted at the B3LYP level of theory (Figure F5 in SI). The dominant charge-transfer process is σ donation from the

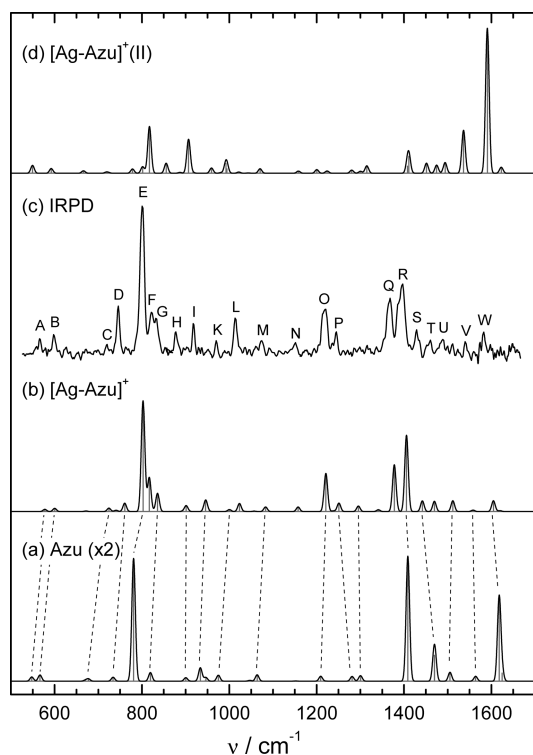


Figure 3. Simulated IR spectra of Azu (a) (multiplied by 2), the global minimum-energy structure $[\text{Ag-Azu}]^+(\text{I})$ (b), and the isomer $[\text{Ag-Azu}]^+(\text{II})$ (d), calculated at the BHPY/augcc-pVTZ level (10 cm^{-1} convolution) compared to the IRPD spectrum of $[\text{Ag-Azu}]^+\cdot\text{Ne}$ (c). The vibrational assignments of the bands A–W are listed in Table T2 in the SI, along with frequencies and IR intensities of the calculated spectra.

delocalized π orbital of Nap (HOMO) to the empty $5s$ orbital of Ag^+ . The reduction of population in the bonding π orbital leads to an expansion of the aromatic ring upon Ag^+ complexation (Figure F2 in SI). Most significantly, the C1C2 and C9C10 bonds in the vicinity of Ag^+ are stretched by 31 and 25 mÅ. On the other hand, as a consequence of the asymmetric location of Ag^+ above the two rings, some CC bonds of the second ring contract somewhat. The circumference of the ring with Ag^+ (8.432 Å) is larger than the other one (8.375 Å), confirming that $\pi \rightarrow \text{Ag}^+$ electron transfer from the first ring dominates. These geometrical changes translate directly into the corresponding frequency shifts induced by Ag^+ complexation (Figure 2, Table T1 in SI). Significantly, the frequencies of all CC stretch and ring modes of Nap are reduced by Ag^+ complexation.

In summary, comparison of the Nap and $[\text{Ag-Nap}]^+$ spectra in Figure 2 unravels two principal effects. First, symmetry reduction from D_{2h} to C_1 substantially increases the complexity of the spectrum as many more modes become IR-active. Second, the presence of the positive charge has a profound impact on the IR intensities even for allowed transitions.^{14,29,30} Comparison of the IR spectra of Nap, $[\text{Ag-Nap}]^+$, and Nap^+ illustrates the effects of systematically increasing the charge on the Nap moiety on vibrational frequencies and IR intensities (Figure F6 in SI). In particular, the IR spectrum of $[\text{Ag-Nap}]^+$ exhibits profound sensitivity to details of the potential energy surface.

The IRPD spectrum of $[\text{Ag-Azu}]^+\cdot\text{Ne}$ was measured from 590 to 1650 cm^{-1} (Figure 3), and the 22 IR bands observed (A–W) are assigned in Table T2 in SI. Similar to $[\text{Ag-Nap}]^+\cdot\text{Ne}$, the

strongest absorptions found at 800 (E) and 1397 cm^{-1} (R) are assigned to the out-of-plane CH bend and CC stretch modes, respectively. The calculations predict two different minima on the $[\text{Ag-Azu}]^+$ potential (Figure 1), and their calculated IR spectra are compared to the measured IRPD spectrum in Figure 3. In the global minimum, $[\text{Ag-Azu}]^+(\text{I})$, Ag^+ binds to C1 of the five-membered ring ($r_{\text{AgC}} = 2.248$ Å) with $D_0 = 198$ kJ/mol (see Figure F7 in SI for all geometrical parameters). The isomer $[\text{Ag-Azu}]^+(\text{II})$, in which Ag^+ binds to C₅ of the six-membered ring ($r_{\text{AgC}} = 2.301$ Å), lies 44 kJ/mol higher in energy. Both Ag^+ binding sites are also the most favorable protonation sites of Azu.²⁹ The calculated IR band positions for $[\text{Ag-Azu}]^+(\text{I})$ show good agreement with the experimental ones and allow for an assignment of all vibrational bands, with a maximum deviation between experimental and calculated frequencies of 30 cm^{-1} (average 12 cm^{-1}). The spectrum calculated for the higher energy $[\text{Ag-Azu}]^+(\text{II})$ isomer differs largely from the experimental one (Figure 3), excluding it from an assignment. The IE of Azu (7.42 eV) is slightly smaller than that of Ag (7.58 eV). Hence, charge transfer in $[\text{Ag-Azu}]^+(\text{I})$ is predicted to be more substantial than that in $[\text{Ag-Nap}]^+$, with only +0.8 versus +0.9 e residing on Ag (Figure F5 in SI). The larger charge transfer in $[\text{Ag-Azu}]^+(\text{I})$ results also in a larger ring expansion and a stronger Ag–PAH bond. The different bonding character in both $[\text{Ag-PAH}]^+$ species is also evident from the prediction that Ag^+ binds to a single C atom in $[\text{Ag-Azu}]^+(\text{I})$ with $r_{\text{AgC}} = 2.25$ Å but to two C atoms in $[\text{Ag-Nap}]^+$ with somewhat longer bonds (2.398 and 2.40 Å). As for $[\text{Ag-Nap}]^+$, Ag^+ complexation of Azu has a strong impact on its structure and IR spectrum (Figure 3). For example, the nearly equal peripheral CC bond lengths of the five-membered ring (1.391 ± 0.001 Å) show strongly alternating behavior in $[\text{Ag-Azu}]^+(\text{I})$ (1.37–1.45 Å), demonstrating that the aromaticity is largely removed upon Ag^+ complexation. These structural changes are again reflected in the vibrational frequencies. For example, the bond elongation of C1C2 (+45 mÅ) results in a red shift in the corresponding CC stretch frequency, $\Delta\nu_8(\text{calc}) = -28$ cm^{-1} and $\Delta\nu_8(\text{exp}) = -48$ cm^{-1} (band S). Similar to $[\text{Ag-Nap}]^+$, the out-of-plane CH bend (ν_{43} , b_2 , band E), in which all H atoms vibrate against all C atoms, shows high IR activity and a large blue shift upon complexation (+36 cm^{-1}).

In conclusion, the analysis of the IRPD spectra of $[\text{Ag-PAH}]^+\cdot\text{Ne}$ complexes provides detailed insight into their structural, vibrational, and electronic properties in the ground electronic state. Complexation of the PAH to Ag^+ is accompanied by substantial charge transfer, leading to structural changes in the PAH, which are directly reflected in the positions and intensities of the IR bands of the complexes compared to those of the bare PAH. The extreme sensitivity of the appearance of the IR spectrum on the details of the charge transfer provides a significant challenge for the proper description by quantum chemical approaches (vide infra). Future target species include larger PAH molecules, other metal ions, and larger metal_x–PAH_y hybrid systems. The experimental approach is also suitable to obtain electronic spectra of these systems to investigate in detail electronic and optical properties of this interesting class of hybrid systems at the molecular level.^{6,9,31}

EXPERIMENTAL SECTION AND COMPUTATIONAL METHODS

IRPD experiments are carried out using an ion trap tandem mass spectrometer,^{16,32} temporarily installed at the FELIX

facility¹⁸ at the FOM Institute Rijnhuizen (The Netherlands). [Ag–PAH]⁺ complexes are continuously generated in a Z-spray ESI source from a 3.6/1 mM PAH/AgNO₃ solution in a 10/1 CH₃OH/H₂O mixture (Figure F1 in SI). The ion beam is collimated in a He-filled radio frequency (rf) ion guide, and [¹⁰⁷Ag–PAH]⁺ ions are mass selected in a quadrupole mass filter, deflected by 90°, and focused into a rf ring electrode ion trap. To allow for continuous ion loading, ion thermalization, and ion–Ne complex formation, the trap is continuously filled with He buffer gas containing 1% Ne at an ion trap temperature of 19 K. Ne-tagged complexes are stabilized through three-body collisions.^{15,16} After filling the trap for 98 ms, all ions are extracted from the trap and focused both temporally and spatially into the center of the extraction region of an orthogonal linear TOF mass spectrometer. Here, the ion packet is irradiated with the IR laser pulse prior to the application of high-voltage extraction pulses and the subsequent measurement of the TOF mass spectrum. IR spectra are recorded by monitoring all ion intensities simultaneously as the laser wavelength is scanned (50–70 measurements per wavelength step). FELIX is operated at 10 Hz with a bandwidth of ~0.2% rms of the central wavelength (2 cm⁻¹ at 10 μm) and average pulse energies of 10 mJ. The photodissociation cross section σ is determined from the relative abundances of parent and photo-fragment ions, I_0 and $I(\nu)$, and the frequency-dependent laser power $P(\nu)$ using $\sigma \sim -\ln[I(\nu)/I_0]/P(\nu)$.

Initial quantum chemical calculations have been carried out at the MP2 and DFT levels using a large variety of functionals with the cc-pVDZ (DFT) and cc-pVTZ (MP2) basis sets and the Stuttgart effective core potential for Ag.³³ The resulting IR spectra and structures for [Ag–Nap]⁺ and [Ag–Azu]⁺ are compiled in Figures F8–F10 in the SI. These test calculations reveal that, although the preferred binding sites of Ag⁺ to the PAH molecules are similar at all theoretical levels, the Ag atom is located slightly outside of the aromatic rings at the DFT level (independent of the functional and basis set, Figure 1), whereas it tends to be inside of the rings at the MP2 level (Figure F10 in SI).²⁸ Surprisingly, the calculated IR spectra in Figures F8–F10 in the SI exhibit a rather high sensitivity to the theoretical level employed, in particular, when also considering the intensities. Moreover, the calculated binding energies strongly depend on the theoretical level (Table T3 in SI). This unusual high sensitivity of the geometry, binding energy, and IR spectral properties is attributed to the subtle effects of the charge transfer occurring in these hybrid complexes composed of constituents with similar ionization energies. Thus, good agreement with experiment is only expected for theoretical approaches, which properly describe the charge transfer. Comparison of the calculated and measured IR spectra in Figures F8–F10 in the SI suggests that MP2 is not performing well. Out of the tested DFT functionals, BHLYP produces the best agreement, and this observation is rationalized by its ability to properly predict the difference of the ionization energies of Ag and the PAH (Table 3 in SI). Test calculations for [Ag–benzene]⁺ at the BHLYP level using basis sets ranging from cc-pVDZ to aug-cc-pVTZ yield binding energies in the range of 145–150 kJ/mol, which agree to within experimental error with the measured dissociation energy of $D_0 = 162 \pm 19$ kJ/mol derived from radiative association kinetics experiments.³⁴ Similar to the binding energies, the calculated IR spectra do not significantly depend on the basis set (Figure F11 in SI). To this end, all further calculations are conducted at the BHLYP/aug-cc-pVTZ level (aug-cc-pVTZ-PP for Ag). Binding energies are corrected for scaled zero-point

vibrational energies. Harmonic vibrational frequencies are scaled by a factor of 0.95, and IR stick spectra are convoluted with a Gaussian profile with 10 cm⁻¹ fwhm. All experimental and theoretical data are reported for the monoisotopic [Ag–PAH]⁺ species.

■ ASSOCIATED CONTENT

Supporting Information. Geometries, charge distributions, calculated IR spectra at various theoretical levels, and peak positions with assignments for PAH, PAH⁺, [Ag–PAH]⁺, and [Ag–PAH]⁺·Ne. This material is available free of charge via the Internet at <http://pubs.acs.org>.

■ ACKNOWLEDGMENT

This work was supported by Technische Universität Berlin (MOSC), Deutsche Forschungsgemeinschaft (FOR 1282, DO 729/5, SFB 546), and the European Community (FP7/2007-2013, grant 226716). We thank the Stichting voor Fundamenteel Onderzoek der Materie (FOM) for beam time at FELIX and the FELIX staff for support and assistance. L.J. thanks the Alexander von Humboldt Foundation for a postdoctoral fellowship.

■ REFERENCES

- (1) Homann, K. H. Fullerenes and Soot Formation — New Pathways to Large Particles in Flames. *Angew. Chem., Int. Ed.* **1998**, *37*, 2435–2451.
- (2) Tielens, A. G. G. M. Interstellar Polycyclic Aromatic Hydrocarbon Molecules. *Annu. Rev. Astron. Astrophys.* **2008**, *46*, 289–337.
- (3) Novoselov, K. S.; Geim, A. K.; Morozov, S. V.; Jiang, D.; Zhang, Y.; Dubonos, S. V.; Grigorieva, I. V.; Firsov, A. A. Electric Field Effect in Atomically Thin Carbon Films. *Science* **2004**, *306*, 666–669.
- (4) Geim, A. K.; Novoselov, K. S. The Rise of Graphene. *Nat. Mater.* **2007**, *6*, 183–191.
- (5) Allen, M. J.; Tung, V. C.; Kaner, R. B. Honeycomb Carbon: A Review of Graphene. *Chem. Rev.* **2010**, *110*, 132–145.
- (6) Martinez, J. I.; Garcia-Lastra, J. M.; Lopez, M. J.; Alonso, J. A. Optical to Ultraviolet Spectra of Sandwiches of Benzene and Transition Metal Atoms: Time Dependent Density Functional Theory and Many-Body Calculations. *J. Chem. Phys.* **2010**, *132*, 044314 and references therein.
- (7) Duncan, M. A. Structures, Energetics and Spectroscopy of Gas Phase Transition Metal Ion–Benzene Complexes. *Int. J. Mass Spectrom.* **2008**, *272*, 99–118.
- (8) Yang, D. S. High-Resolution Electron Spectroscopy of Gas-Phase Metal–Aromatic Complexes. *J. Phys. Chem. Lett.* **2011**, *2*, 25–33.
- (9) Buchanan, J. W.; Grieves, G. A.; Flynn, N. D.; Duncan, M. A. Photodissociation of Silver–Coronene Cluster Cations. *Int. J. Mass Spectrom.* **1999**, *187*, 617–624.
- (10) Szczepanski, J.; Wang, H. Y.; Vala, M.; Tielens, A.; Eyler, J. R.; Oomens Infrared Spectroscopy of Gas-Phase Complexes of Fe⁺ and Polycyclic Aromatic Hydrocarbon Molecules. *Astrophys. J.* **2006**, *646*, 666–680.
- (11) Simon, A.; Joblin, C.; Polfer, N.; Oomens, J. Infrared Spectroscopy of [XFeC₂₄H₁₂]⁺ (X = C₃H₅, C₅(CH₃)₅) Complexes in the Gas Phase: Experimental and Computational Studies of Astrophysical Interest. *J. Phys. Chem. A* **2008**, *112*, 8551–8560.
- (12) Lee, J. S.; Krasnokutski, S. A.; Yang, D. S. High-Resolution Electron Spectroscopy, Preferential Metal-Binding Sites, and Thermochemistry of Lithium Complexes of Polycyclic Aromatic Hydrocarbons. *J. Chem. Phys.* **2011**, *134*, 024301.
- (13) Takino, M.; Daishima, S.; Yamaguchi, K.; Nakahara, T. Determination of Polycyclic Aromatic Hydrocarbons by Liquid Chromatography-Electrospray Ionization Mass Spectrometry Using Silver Nitrate as a Post-Column Reagent. *J. Chromatogr., A* **2001**, *928*, 53–61.

(14) Knorke, H.; Langer, J.; Oomens, J.; Dopfer, O. Infrared Spectra of Isolated Protonated Polycyclic Aromatic Hydrocarbon Molecules. *Astrophys. J. Lett.* **2009**, *706*, L66–L70.

(15) Brümmer, M.; Kaposta, C.; Santambrogio, G.; Asmis, K. R. Formation and Photodepletion of Cluster Ion–Messenger Atom Complexes in a Cold Ion Trap: Infrared Spectroscopy of VO^+ , VO_2^+ , and VO_3 . *J. Chem. Phys.* **2003**, *119*, 12700–12703.

(16) Goebbert, D. J.; Wende, T.; Bergmann, R.; Meijer, G.; Asmis, K. R. Messenger-Tagging Electrosprayed Ions: Vibrational Spectroscopy of Suberate Dianions. *J. Phys. Chem. A* **2009**, *113*, 5874–5880.

(17) Valle, J. J.; Eyler, J. R.; Oomens, J.; Moore, D. T.; van der Meer, A. F. G.; von Helden, G.; Meijer, G.; Hendrickson, C. L.; Marshall, A. G.; Blakney, G. T. Free Electron Laser-Fourier Transform Ion Cyclotron Resonance Mass Spectrometry Facility for Obtaining Infrared Multiphoton Dissociation Spectra of Gaseous Ions. *Rev. Sci. Instrum.* **2005**, *76*, 023103.

(18) Oepts, D.; van der Meer, A. F. G.; van Amersfoort, P. W. The Free-Electron-Laser User Facility FELIX. *Infrared Phys. Technol.* **1995**, *36*, 297–308.

(19) Okumura, M.; Yeh, L. I.; Lee, Y. T. The Vibrational Predissociation Spectroscopy of Hydrogen Cluster Ions. *J. Chem. Phys.* **1985**, *83*, 3705–3706.

(20) Bieske, E. J.; Dopfer, O. High-Resolution Spectroscopy of Cluster Ions. *Chem. Rev.* **2000**, *100*, 3963.

(21) Piest, H.; von Helden, G.; Meijer, G. Infrared Spectroscopy of Jet-Cooled Cationic Polyaromatic Hydrocarbons: Naphthalene⁺. *Astrophys. J.* **1999**, *520*, L75.

(22) Linstrom, P. J.; Mallard, W. G. *NIST Chemistry WebBook*; NIST Standards and Technology: Gaithersburg MD, 2011; see: <http://webbook.nist.gov>.

(23) Lagutschenkov, A.; Sinha, R. K.; Maitre, P.; Dopfer, O. Structure and Infrared Spectrum of the Ag^+ –Phenol Ionic Complex. *J. Phys. Chem. A* **2010**, *114*, 11053–11059.

(24) Chakraborty, S.; Dopfer, O. Infrared Spectrum of the Ag^+ –(Pyridine)₂ Ionic Complex: Probing the Interactions in Artificial Metal-Mediated Base Pairing. *ChemPhysChem* **2011**, *12*, 1999–2008.

(25) Orgel, L. E. Stereochemistry of Metals of the B Sub-Groups. I. Ions with Filled d-Electron Shells. *J. Chem. Soc.* **1958**, 4186–4190.

(26) Yousef, A.; Shrestha, S.; Viehland, L. A.; Lee, E. P. F.; Gray, B. R.; Ayles, V. L.; Wright, T. G.; Breckenridge, W. H. Interaction Potentials and Transport Properties of Coinage Metal Cations in Rare Gases. *J. Chem. Phys.* **2007**, *127*, 154309.

(27) Dargel, T. K.; Hertwig, R. H.; Koch, W. How Do Coinage Metal Ions Bind to Benzene? *Mol. Phys.* **1999**, *96*, 583–591.

(28) Yi, H. B.; Lee, H. M.; Kim, K. S. Interaction of Benzene with Transition Metal Cations: Theoretical Study of Structures, Energies, and IR Spectra. *J. Chem. Theory Comput.* **2009**, *5*, 1709–1717.

(29) Zhao, D.; Langer, J.; Oomens, J.; Dopfer, O. Infrared Spectra of Protonated Polycyclic Aromatic Hydrocarbon Molecules: Azulene. *J. Chem. Phys.* **2009**, *131*, 184307.

(30) Defrees, D. J.; Miller, M. D.; Talbi, D.; Pauzat, F.; Ellinger, Y. Theoretical Infrared Spectra of Some Model Polycyclic Aromatic-Hydrocarbons — Effect of Ionization. *Astrophys. J.* **1993**, *408*, 530–538.

(31) Simon, A.; Joblin, C. Photodissociation of $[\text{Fe}_x(\text{C}_{24}\text{H}_{12})_y]^+$ Complexes in the PIRENEA Setup: Iron-Polycyclic Aromatic Hydrocarbon Clusters as Candidates for Very Small Interstellar Grains. *J. Phys. Chem. A* **2009**, *113*, 4878–4888.

(32) Goebbert, D. J.; Meijer, G.; Asmis, K. R. 10 K Ring Electrode Trap—Tandem Mass Spectrometer for Infrared Spectroscopy of Mass Selected Ions. *AIP Conf. Proc.* **2009**, *1104*, 22.

(33) Ahlrichs, R.; Bär, M.; Häser, M.; Horn, H.; Kölmel, C. Electronic Structure Calculations on Workstation Computers — The Program System Turbomole. *Chem. Phys. Lett.* **1989**, *162*, 165–169.

(34) Ho, Y. P.; Yang, Y. C.; Klippenstein, S. J.; Dunbar, R. C. Binding Energies of Ag^+ and Cd^+ Complexes from Analysis of Radiative Association Kinetics. *J. Phys. Chem. A* **1997**, *101*, 3338–3347.